Derivation of site-specific relationships between hydraulic parameters and p-wave velocities based on hydraulic and seismic tomography

Brauchler, R.[1], Doetsch, J. [1,2], Dietrich, P. [3], Sauter, M. [4]

[1] ETH Zurich, Department of Earth Sciences, Sonneggstrasse 5, 8092 Zurich, Switzerland

[2] *now at:* Earth Sciences Division, Lawrence Berkeley National Laboratory, One Cyclotron Road, Berkeley, CA 94720

[3] UFZ, Helmholtz Centre for Environmental Research, Department Monitoring and Exploration Technologies, Permoserstrasse 15, 04318 Leipzig, Germany

[4] Geoscientific Centre, University of Göttingen, Goldschmidtstraße 3, 37077 Göttingen, Germany

Abstract:

In this study, hydraulic and seismic tomographic measurements were used to derive a site-specific relationship between the geophysical parameter p-wave velocity and the hydraulic parameters, diffusivity and specific storage. Our field study includes diffusivity tomograms derived from hydraulic travel time tomography, specific storage tomograms, derived from hydraulic attenuation tomography, and p-wave velocity tomograms, derived from seismic tomography. The tomographic inversion was performed in all three cases with the SIRT (Simultaneous Iterative Reconstruction Technique) algorithm, using a ray tracing technique with curved trajectories. The experimental set-up was designed such that the p-wave velocity tomogram overlaps the hydraulic tomograms by half. The experiments were performed at a well-characterized sand and gravel aquifer, located in the Leine River valley near Göttingen, Germany. Access to the shallow subsurface was provided by direct-push technology. The high spatial resolution of hydraulic and seismic tomography was exploited to derive representative site-specific relationships between the hydraulic and geophysical parameters, based on the area where geophysical and hydraulic tests were performed. The transformation of the p-wave velocities into hydraulic properties was undertaken using a k-means cluster analysis. Results demonstrate that the combination of hydraulic and geophysical tomographic data is a promising approach to improve hydrogeophysical site characterization.

1. Introduction

Tomographic geophysical methods show a great potential in providing information on the design and parameterization of conceptual and numerical models, allowing the quantitative prediction of flow and transport processes in the subsurface [Day-Lewis and Lane, 2004]. From geophysical tomograms, structural information to delineate zones with constant hydraulic properties in a numerical flow and transport model can be exploited. [e.g. Hyndman and Harris, 1996]. Several advanced approaches in delineating zones of constant geophysical properties were developed based on the joint inversion of multiple geophysical data sets by several researchers [e.g. Hyndman et al.,1994; Dietrich et al., 1998; Gallardo and Meju, 2003; Tronicke et al., 2004; Linde et al., 2006a; Cardiff and Kitanidis, 2009; Doetsch et al., 2010]. The hydraulic properties of the estimated zones can be inferred from core data, hydraulic tests or tracer test data. However, the key assumption regarding these structural hydrogeophysical inversion approaches is that the individual zones have approximately constant hydrogeological and geophysical properties.

Over the last decade and a half, several research groups started to work on developing coupled hydrogeophysical inversion schemes based on tomographic geophysical methods. Coupled hydrogeophysical inversion focuses on estimating hydrogeological parameters and their spatial distribution directly from geophysical measurements. Usually, petrophysical relationships and models are used to transform a resulting geophysical parameter distribution into an image of hydraulic parameters. Often coupled hydrogeophysical inversion schemes can eliminate the need to construct images of geophysical property distributions [Ferre et al., 2009]. Hinnell et al. [2010] give an excellent overview about the workflow of coupled

inversion schemes. Hyndman et al. [2000], for example, combined densely sampled cross-well tomographic slowness estimates with hydraulic information derived from core data and pumping tests in order to estimate hydraulic conductivity fields that minimize the discrepancy/inconsistency/ambiguity between tracer and drawdown data. Based on this work, Linde et al. [2006b] presented a methodology to estimate hydraulic conductivity fields using radar tomograms without assuming that the petrophysical relationships are constant across interpreted velocity zones, and without assuming that the geophysical and hydrogeological properties are constant within the zones. However, the results are based on the assumption that a relationship between radar velocity and hydraulic conductivity exists. Kowalsky et al. [2004] developed an inversion scheme to determine water saturation based on radar velocities and hydraulic point information using a known, rather than a site-specific relationship. The approach was tested by different numerical experiments. Kowalsky et al. [2005] applied a modified approach estimating the petrophysical relationship as part of the inverse problem and successfully applied the method to field data.

Another type of approach combining geophysical, geological and hydrogeological data to estimate the spatial parameter field comprises geostatistical methods [Cassiani et al., 1998; Hubbard et al., 1999; Yeh et al., 2002; Chen et al., 2001; 2004].

Virtually all hydrogeophysical investigations are based on a relationship that links geophysical parameters with hydrogeophysical parameters. There are several petrophysical relationships, such as Topp´s equations [Topp et al., 1980] and Archie´s law [Archie, 1942], which are applied intensively to determine the water saturation. However, Yeh at al., 2000 observed significant variability of the electrical

resistivity-moisture relation in their field samples. Based on theoretical analysis and numerical experiments they could show that the spatially varying relationship between electrical resistivity and moisture content can influence the significance of moisture monitoring results derived from the estimated change in the electrical resistivity. Liu and Yeh, 2004 supports these findings and concluded that additional hydrological a priori information next to electrical resistivity measurements are needed under field conditions in order to yield hydrological realistic inversion results.

Other relationships, e.g. between seismic velocities or radar velocities and hydraulic conductivity, are likely non-unique. This non-uniqueness leads to the derivation of site-specific relationships between geophysical and hydraulic parameters. This is in accordance with Hyndman and Tronicke [2005], who stated: “Estimating the relation between geophysical and hydrogeologic parameters is a site-specific endeavor, since no general relation is expected.” The estimation of site-specific relationships can be very difficult and even erroneous due to the different spatial resolution of available geophysical and hydraulic data.

Usually, geophysical tomographic reconstructions show a high spatial resolution in two or even in three dimensions. Classical hydrogeological approaches, however, appear to have difficulties providing high-resolution parameter estimates [Butler, 2005]. Pumping tests lead to reliable estimates in hydraulic conductivity and storage but the resulting hydraulic properties represent spatial averages over a large aquifer volume. Slug tests, however, provide information about the hydraulic parameters in the immediate vicinity of the well. The resolution of hydraulic testing in a vertical direction can be even increased by using multi-packer systems [e.g. Melville et al, 1991; Butler 1998; Brauchler et al., 2010]. Lateral changes in hydraulic parameters

can be derived from hydraulic cross-well tests. It has to be emphasized that the estimated hydraulic properties derived from type curve analysis, assuming a homogeneous parameter distribution, do not reflect a uniformly weighted average, but the weight depends on the test and observation interval and the heterogeneity of the subsurface [Wu et al., 2005]. Thus, the spatial assignment of the hydraulic properties is non-unique [Leven and Dietrich, 2006] and the derivation of site-specific relationships between hydraulic and geophysical parameter reconstruction could be biased.

However, several research groups are working on a new hydraulic investigation technique, termed *hydraulic tomography* that has the potential to yield information on spatial variation of hydraulic properties with a resolution comparable to the spatial resolution of geophysical tomographic investigations [e.g. Gottlieb and Dietrich, 1995; Yeh and Liu, 2000; Vasco and Karasaki, 2001; Karasaki et al., 2000; Bohling et al., 2002; Brauchler et al., 2003; Zhu and Yeh; 2005; 2006; Straface et al., 2007; Ni and Yeh, 2008; Xiang et al., 2009; Yin and Illmann, 2009; Illman et al., 2010]. Hydraulic tomography consists of a series of short-term pumping or slug tests. Varying the location of the source stress (pumping or slug interval) and the receivers (pressure transducers) generates streamline patterns that are comparable to the crossed ray paths of a seismic tomography experiment [Butler et al., 1999]. One of the first tomographic measurement arrays in the field were implemented by Hsieh et al. [1985]. Due to the high spatial resolution of the hydraulic and geophysical tomographic images, a representative site-specific relationship can be derived over an area where geophysical and hydraulic tests are performed, if such a relationship exists.

In this study, the potential of hydraulic tomography to derive a site-specific relationship between hydraulic parameters and p-wave velocity for the well-characterized Stegemühle site near Göttingen, Germany, will be assessed. The hydraulic tomographic inversion presented in Brauchler et al. [2011] consists of 196 pressure cross-well interference slug tests performed between five wells, in which the positions of the sources (injection ports) and the receivers (observation ports), isolated with double packer systems, were varied between tests. The database for the seismic tomography experiments comprises four seismic planes overlapping half the hydraulic tomograms. The derivation of a site specific relationship, based on k-means clustering [McQueen, 1967], enabled us to identify the spatial position of two zones and their average hydraulic properties within the reconstructed p-wave velocity tomograms.

2. Overview of the Stegemühle Site

The Stegemühle site is located in the Leine valley, close to Göttingen, Germany and has been characterized extensively by geophysical wellbore logging, refraction seismic and hydraulic testing. The infrastructure of the site consists of a network of 26 wells, comprising 1”, 2”, 6” and multi-chamber wells screened over the whole aquifer thickness (Figure 1). The 6” wells were drilled with a top drive drilling rig, whereas all other wells were installed using direct-push (DP) technology. The DP-technology uses a hydraulic hammer, supplemented with the weight of the direct-push unit to push drive rods down to the desired depth of the projected well [e.g. Dietrich and Leven, 2006]. The well casing, consisting of high-density polyethylene (HDPE) pipes and slotted screens, is then lowered into the drive rods (inner

diameter: 0.067 m, outer diameter 0.083 m). By retracting the drive rods, the formation is allowed to collapse back against the HDPE pipes.

The structural composition of the braided river sediments was characterized by surface refraction seismic, gamma ray logging and direct-push electrical conductivity logging. For selected wells, cores are recovered to calibrate the recorded logs. The aquifer thickness varies between 2-2.5 m and consists of intercalated sand and gravel layers. A confining unit that consists of silt and clay overlies the aquifer. The thickness of the confining unit varies between 3-3.5 m [Brauchler et al., 2010]. The cores displayed, that the aquifer material at the Stegemühle site shows a sharp transition from one behavior to another [Hu, 2011]. The sharp transition can be explained by the complexity of depositional and erosional processes in braided river systems [Huggenberger and Regli, 2006].

The hydraulic characterization is based on pumping and cross-well slug interference tests. Hydraulic conductivity estimates, derived from multi-level single-well slug tests, performed at five to seven different depths in each 2" well, vary between 10^{-4} ms^{-1} and 5×10^{-3} ms^{-1}. Brauchler et al. [2010] determined vertical changes in hydraulic conductivity and specific storage with multi-level cross-well interference slug testing between the five wells (P2.5/M25, P0/M27.5, PM2.5/M25, P0/M22.5 and P0/M25) arranged in a five-star configuration (Figure 1). The estimated hydraulic conductivity values decrease from approximately 10^{-3} ms^{-1}, close to the bottom, to approximately 10^{-4} ms^{-1}, at the top of the aquifer and the specific storage distribution shows an opposite behavior. The specific storage values increase from approximately 10^{-5} m^{-1} close to the bottom of the aquifer to approximately 10^{-3} m^{-1} at the top of the aquifer.

Brauchler et al. [2011] inverted the cross-well interference slug tests with a travel time and attenuation based inversion scheme. They reconstructed the diffusivity and specific storage distribution between the wells in two and three dimensions. In Figure 2, the reconstructed three-dimensional hydraulic diffusivity distribution and specific storage tomograms are shown. Note that Figure 2 is adapted from the work performed by Brauchler et al. [2011]. The limited number of injection and observation intervals prevented us from resolving small-scale (10 cm in size) variability of hydraulic conductivity. This is in accordance with findings from Hu et al. [2011]. They performed a numerical case study based on data derived from an aquifer analog outcrop study and could show that with a reasonable number of source and receivers, it is not possible to reconstruct small-scale variability (10 cm in size) using the travel time based inversion approach.

Brauchler et al. [2012] recorded a suite of short-term pumping tests, using a tomographical measurement array between well P0/M25 and multi-chamber well PM5/M17.5. The reconstructed hydraulic diffusivity distribution, based on hydraulic travel time inversion, shows a similar pattern, as the diffusivity tomogram illustrated in Figure 2, with the highest values close to the bottom of the aquifer. The comparison of the travel time inversion results with the results based on straight line analysis (solution of Cooper and Jacob, [1946]) have shown that the hydraulic parameters estimated with a straight analysis are dominated by the high permeability layer close to the bottom of the aquifer. The recorded inversion results indicate that the combination of hydraulic travel time and hydraulic attenuation tomography allows the reconstruction of the diffusivity and storage distribution in two and three dimensions, with a resolution and accuracy superior to that possible with type curve/straight line analysis.

The hydraulic characterization of the site showed that the shallow aquifer, with a thickness of two meters, is ideally suited to develop and perform new investigation techniques. The thinness of the aquifer allows for the minimization of the logistical and technical requirements of complex hydraulic testing and simplifies the validation of new investigation techniques with conventional investigation techniques.

In the following, we exploit the earlier work described above and propose an approach combining hydraulic and seismic tomography, as well as direct-push (DP) technology. These three techniques complement one another as described: (1) Hydraulic tomograms are well suited to derive site-specific relationships between hydraulic parameters and indirect geophysical measurements because changes in hydraulic properties can be reconstructed in horizontal, as well as in lateral direction with high spatial resolution. (2) The integration of hydraulic and seismic tomography allows for an easy enlargement of the investigation area, since geophysical cross-well measurements can be performed faster than hydraulic tests, and thus, a larger area can be covered in one array. (3) The characterization of larger areas with hydraulic and seismic cross-well tests has been limited by the need for wells that are arranged and designed in a way that hydraulic multi-level cross-well, as well as seismic cross-well, experiments can be performed. That limitation, however, can be readily overcome in unconsolidated formations by exploiting the access to the shallow subsurface provided by DP technology. DP technology can be used to install observation points with different types of casing at positions most advantageous for a particular study and an option to reposition measurement points between tests based on the former results.

3. Seismic tomographic measurements

For the performance of seismic cross-well measurements, four non-permanent direct-push wells were installed and used as test wells (Figure 1). The installation of the wells consists of a shielded screen at the lower end of the direct-push tool string. The used screen, with an inner diameter of 0.016 m, was originally designed for water sampling or slug testing [Butler et al., 2002]. The temporary wells were chosen as source wells because conventional wells are likely to be damaged by the action of the sparker source. For test initiation, a modified p-wave sparker probe, SBS 42, adapted to small diameter wells in combination with an electric surge generator and a remote control unit was used.

For the initiation of the seismic experiments, the shielded screen at the lower end of the direct-push tool string was pushed down to the position of the deepest test interval. After having reached the selected depth, the shielded screen tool was exposed and a cross-well seismic test is initiated. Subsequently, the direct-push tool string was pulled back in order to perform the test at different depths.

The seismic signal was recorded with a hydrophone string, consisting of ten single hydrophones, placed in the center well P0/M25 of the five-star configuration, with a spacing of 0.24 m. The individual hydrophones have a diameter of 0.02 m and a preamplifier of 20 dB. The small distance of 5 m between source and receiver well and the preamplifier lead to very strong signals with the result that the seismic waveforms were clipped. However, the first arrivals could be clearly identified (Figure 3). The advantage of using non-permanent direct-push wells as test wells is a low-

cost installation in terms of time effort and finances. It has to be mentioned that a possible vertical deviation of the wells can lead to errors in the inversion results. An experienced technician team can minimize such deviation but it cannot be fully excluded.

In total we recorded data on four seismic planes (profiles) between the four non-permanent direct-push wells and the center well P0/M25 of the five-star configuration. Therefore, the data set for each plane consists of ten injection and ten observation positions. The source–receiver configurations are displayed as pink lines in Figure 4. The black lines, illustrate the measured configurations, as well as the spatial position of the test and observation intervals of the cross-well slug interference tests. The four seismic tomograms are half overlapping, with the area investigated by hydraulic tomography. We used the hydraulic inversion results, based on these measured configurations, to derive a site-specific relationship for the Stegemühle site between p-wave velocity and the hydraulic parameters diffusivity and specific storage.

4. Estimation of the site-specific relationship

In this section we provide a short review about the hydraulic travel time inversion, hydraulic attenuation inversion and seismic travel time inversion, followed by a description of the derivation of a sites-specific relationship between hydraulic parameters and p-wave velocity for the Stegemühle site. The inversion results constitute the basics for the derivation of a representative site-specific relationship. The hydraulic tomographic inversion results employed in this study are based on earlier work described by Brauchler et al. [2010, 2011].

The work proposed by Vasco et al. [2000] is the starting point of the hydraulic tomographic inversion. They proposed an inversion scheme that follows the procedure of seismic ray tomography and is based on the transformation of the transient ground water flow equation into the eikonal equation using an asymptotic approach [Virieux et al. 1994]. The eikonal equation can be solved with ray tracing techniques or particle tracking methods, which allow for the calculation of pressure propagation along trajectories.

The key element of the hydraulic inversion are two line integrals: (a) A travel time integral which relates the travel time of transient signal with a Dirac source at the origin to the diffusivity (*D)* distribution between source and receiver and (b) an attenuation integral which relates the attenuation of a pressure signal with a Dirac source signal at the origin to the specific storage (S_s) distribution.

(a) Travel time integral:

$$\sqrt{t_{\alpha,d}} = \frac{1}{\sqrt{6 f_{\alpha,d}}} \int_{x_1}^{x_2} \frac{ds}{\sqrt{D(s)}} . \tag{1}$$

$t_{\alpha,d}$ is the travel time (arrival time) of a selected point of the signal from the point x_1 (source) to the observation point x_2 (receiver) and D is the diffusivity as a function of arc-length along the propagation path (s) and $f_{\alpha,d} = t_{peak}/t_{\alpha,d}$ the related transformation factor. t_{peak} is defined as the peak time of the recorded transient pressure curve and the subscript $_d$ stands for a Dirac source. The transformation factor allows to relate any recorded travel time $t_{\alpha,d}$ with the diffusivity D and is defined as follows:

$$f_{\alpha,d} = -W\left(-\frac{\left(\frac{h_d(r,t)}{h_d(r,t_{peak})} \right)^{\frac{2}{3}}}{e} \right) \tag{2}$$

W stands for Lambert's *W function* and $h_d(r,t)$ describes the hydraulic potential as function space and time. Brauchler et al. [2003] presents the derivation of the transformation factor in detail.

b) Attenuation integral:

$$\left(\frac{h(x_2)}{H_0}\right)^{-\frac{1}{3}} = B^{-\frac{1}{3}} \int_{x_1}^{x_2} \left(\frac{1}{S_s(s)}\right)^{-\frac{1}{3}} ds \tag{3}$$

The attenuation of the hydraulic signal is expressed by the initial displacement H_0 and the hydraulic head $h(x_2)$ at the observation interval and S_s is the specific storage as a function of arc-length along the propagation path (s). The parameter B was introduced to simplify equation (3) and is defined as follows:

$$B = \frac{\pi r_c'^2}{\sqrt{\left(\frac{2\pi}{3}\right)^3}} \exp\left[-\frac{3}{2}\right] \tag{4}$$

Here r_c is the casing radius. Brauchler et al. [2011] described in detail the derivation of the attenuation integral.

In seismic tomography a similar relationship exists, which can be expressed as a line integral. The line integral relates the travel time t of a seismic pulse to the inverse of the velocity ($1/v$) as a function of arc-length along the propagation path (s). The inverse of the velocity is termed slowness.

$$t = \int_{x_1}^{x_2} \frac{ds}{v(s)} \tag{5}$$

The similarity of all three line integrals allows the application of the same inversion algorithms. The inversion was performed in all three cases with the SIRT (Simultaneous Iterative Reconstruction Technique) algorithm [Gilbert, 1972]. The algorithm allows for the application of ray tracing techniques with either straight or curved ray paths and trajectories, respectively. We used curved ray paths to handle the large travel time contrasts of several orders of magnitude in hydraulic tomography [Brauchler et al., 2007]. The curved ray paths are computed based on the ray tracing algorithm developed by Um and Thurber [1987]. Tests with the LSQR-based inversion code of Doetsch et al. [2010] recovered the same main features as the SIRT inversions, when using logarithmic transformations for both data and model parameters in the hydraulic tomography.

For the seismic travel time inversion, as well as for the hydraulic and attenuation travel time inversion a homogeneous starting model was used. The starting values for the velocity/attenuation fields are derived from the mean values of the measured source-receiver-combinations. The cell size of 0.35 m × 0.4 m is the same for all three tomograms.

The main steps to derive a site-specific relationship between hydraulic parameters and p-wave velocity are described in the following and summarized in a flowchart, which is displayed in Figure 5:

Step 1: Reconstruction of the diffusivity, specific storage and p-wave tomograms using the inversion scheme described above.

Step 2: Differentiation between hydrogeological units characterized by a significant diffusivity, specific storage and p-velocity contrast and determination of the number of

such significant hydrogeological features apparent in the tomograms. If no relationship between hydraulic tomograms and geophysical tomograms can be recognized, the investigation has to be stopped at this step. The approach is limited to sites where a relationship between hydraulic and geophysical parameters exists.

Step 3: Zonation of the area, which is covered by all three tomograms. In this study, the area is located between the wells P0/M22.5 and P0/M27.5, as well as the area between P2.5/M25 and PM2.5/M25. The zonation is performed by k-means cluster analysis [McQueen, 1969]. The clusters were calculated using normalized Euclidian distances (root mean squared distances) without using any spatial adjacency. Prior to the cluster analysis the used parameters, diffusivity, specific storage and p-wave velocity, were standardized (mean of zero, standard deviation of one) in order to account for the different units. The number of clusters was chosen equivalent to the number of the determined hydrogeological features estimated in step 2. Cluster analysis was applied successfully in several studies to objectively identify major common trends and groupings in various combinations of hydraulic and geophysical tomographic data [Eppstein and Dougherty, 1998*;* Tronicke et al., 2004; Paasche et al., 2006; 2010; Dietrich and Tronicke, 2009; Doetsch et al., 2010b, Brauchler et al., 2011].

Step 4: Assignment of an average value for specific storage, diffusivity and p-wave velocity to each cluster. Therefore, the arithmetic means of the specific storage, diffusivity and p-wave velocity of the cells, assigned to the respective cluster, are calculated.

Step 5: Zonation of the area, where only information about the p-wave velocities is available. The zonation is performed by calculating the difference between the p-wave velocity for each single cell and the p-wave velocity of the clusters estimated in step 4. The cell is assigned to the cluster, which shows the smallest difference.

Step 6: Verification if the estimated zoned parameter field is consistent with the original hydraulic and geophysical data. Therefore, a second hydraulic travel time, hydraulic attenuation and seismic travel time inversion, using the zonation derived from the k-means cluster analysis as constraints, is performed.

5. Results

The derivation of a site-specific relationship between hydraulic parameters and p-wave velocity for the Stegemühle site are based on the diffusivity, specific storage and p-wave velocity tomograms illustrated in Figures 6 and 7. The procedure described above is performed jointly for the tomograms recorded in (a) North–South direction and the tomograms in (b) West–East direction.

The comparison of the tomograms illustrated in Figures 6 and 7 indicates that the p-wave velocity tomogram is positively related to the specific storage and negatively correlated to the diffusivity distribution. The correlation coefficient for the tomograms recorded in North–South direction between p-wave velocity and the logarithm of diffusivity is -0.63 and between p-wave velocity and logarithm of specific storage it is 0.55. For the tomograms recorded in West–East direction the calculated correlation coefficients are similar. A correlation coefficient of -0.69 between p-wave velocity and

the logarithm of diffusivity and a correlation coefficient of 0.68 between p-wave velocity and logarithm of specific storage were determined.

The respective scatterplots, displayed in Figure 8, indicate, like the calculated correlation coefficients that the p-wave velocity is negatively correlated to diffusivity and positively correlated to specific storage.

For hydrogeophysical investigations based on the combination of geophysical and conventional hydraulic methods, correlation coefficients or scatterplots are often the only way to evaluate the relationship between geophysical and hydraulic properties. However, the high spatial resolution of hydraulic and geophysical tomograms allows for assessing in addition, whether at all and to what extent and detail the most important features are imaged in both tomograms. Hence, it is possible to determine the significance of hydrogeophysical investigations in the identification of hydraulically important features, such as preferential flow paths or barriers influencing flow and solute transport. We performed a variogram analysis in order to show objectively the spatial correlation structures of the diffusivity, specific storage and p-wave velocity tomograms (Figure 9). For all variograms a Gaussian model was selected. The Gaussian model, with its parabolic behavior at the origin, represents very smoothly varying properties. The smoothly varying properties can be explained by the used inversion technique. The SIRT algorithm applied in this study leads to smoother parameter reconstructions in comparison to other series expansion inversion methods, because the incremental corrections are applied by averaging the incremental correction of each single cell after all trajectories have been analyzed (e.g. Dines and Little, 1979). The range of the variograms displayed in Figure 9 is between 0.7 and 0.9. The similarity of the variograms and the comparable statistics

reveals their spatial correlation structures. Having considered the above statistical quality criteria, the following results can be summed up:

(a) Tomograms in North–South direction: The lower part of the diffusivity and the specific storage tomogram is characterized by higher diffusivity values of approximately 10 m/s^2 and lower specific storage values of approximately 10^{-4} m^{-1}, in comparison to the upper part. With increasing height, the diffusivity values decrease to about 1 m/s^2 and the specific storage values increase by one order of magnitude, to a maximum value of 10^{-3} m^{-1}, respectively. Between the wells P2.5/M25 and PM2.5./M25, the p-wave velocity tomogram shows a similar pattern. The lower part of the tomogram is characterized by low p-wave velocities between 2.2 km/s and 2.25 km/s. Closer to the top of the tomogram the velocities increase to 2.35 km/s. The similar pattern of the three tomograms indicates, along with the estimated correlation coefficients and the variogram analysis, is evidence of a site-specific relationship between p-wave velocity and the hydraulic parameters diffusivity and specific storage. For the interpretation of the hydraulic tomograms in terms of groundwater flow and solute transport, it is important to question whether or not the higher diffusivity/low specific storage zone at the bottom extends beyond the area to the left of well P2.5/M25 and across the area to the right of well PM2.5/M25.

b) Tomograms in West–East direction: Between well P0/M25 and well P0/M27.5 the hydraulic tomograms, displayed in Figure 7a and b, show a similar pattern as the hydraulic tomograms recorded in North-South direction. The right section of the hydraulic tomograms is characterized by diffusivity values ranging between 7 m/s^2 and 10 m/s^2 and specific storage values between 10^{-4} m^{-1} and 3×10^{-4} m^{-1} close to the bottom of the tomograms. At the top of the tomograms the diffusivity values vary

between 1 m/s^2 and 2 m/s^2 and the specific storage values vary between 7×10^{-4} m^{-1} and 10^{-3} m^{-1}. The most significant features in the hydraulic tomograms are the lateral changes. Between well P0/M22 and well P0/M25 the high diffusivity/low specific storage zone pinches out. The pinching out of this zone, characterized by low p-wave velocities between 2.15 km/s and 2.18 km/s, can be also recognized in the p-wave velocity tomogram. For the interpretation of the hydraulic tomograms it is important to know whether the high diffusivity/low specific storage zone stretches out over the area right of well P0/M27.5.

In order to answer these questions we generated two zones based on the tomograms recorded in North–South and West–East direction to derive a site-specific relationship using the zonation approach described in section 4. The zonation approach is introduced jointly for all tomograms. The number of the cluster is chosen in accordance with the number of significant hydrogeological features that could be identified reliably from the diffusivity tomograms and specific storage tomograms, as well as in the p-wave velocity tomogram.

The zoned tomogram recorded in North–South direction displayed in Figure 6d, shows that the zone at the lower part of the tomogram is pinching out close to the well P2.5/M25. In the other direction, the thickness of the zone decreases without any pinching out. The zoned tomogram recorded in West–East direction, illustrated in Figure 7, displays the pinching out of the high diffusivity/low specific storage between well P0/M25 and well P0/M22.5. It is difficult to answer whether or not this zone extends beyond the area to the right of well P0/M27.5. The zoned tomogram indicates that the high diffusivity/low specific storage zone continues to the right and ascends towards the aquifer top.

The range of the hydraulic conductivity and specific storage displayed by zone 1 and zone 2 varies between 10^{-3} m/s and 6×10^{-4} m/s and 2×10^{-4} 1/m and 8×10^{-4} 1/m, respectively. These values agree with the hydraulic property estimates derived from type curve analysis [Brauchler et al. 2010]. The range of the hydraulic properties of the two zones has to be smaller than the range of the values derived from type curve analysis, because the two zones display values integrated over half of the model domain.

For the verification of the zonation approach, we applied the procedure proposed by Doetsch et al. [2010]. They suggested that for field data with unknown zone geometries and parameters, the zonation must be judged on the basis of the root means square residual error (RMSE) and by visual inspection. Hence, we performed a second hydraulic travel time, hydraulic attenuation and seismic travel time inversion using the zonation derived from the k-means cluster analysis as constraints. Thereby the parameters within zone 1, representing the high diffusivity/low specific storage zone close to the bottom of the aquifer was kept constant. In Table 1, the RMSE of the hydraulic travel time, hydraulic attenuation, and seismic travel time inversions with and without constrain are listed for the hydraulic tomograms after five and for the p-wave velocity tomogram after 10 iteration steps. It is not surprising that the RMSE of the inversions, without any constraints, is smaller than the RMSE of the inversion with constraints.

However, the comparison of the RMSE shows that the differences are small with respect to the arithmetic mean of the measured (a) p-wave travel times of 2.31 µs, (b) hydraulic travel times of 2.09 s and (c) the attenuation ratio of 0.20. Beyond this,

the reconstructed parameter estimates within zone 2 with and without constraints are comparable. The small difference of the RMSE based on the inversion with and without constraints, respectively, and the fact that the tomograms with constraints exhibit no artifact in zone 2 supports the performed zonation approach.

6. Summary and Conclusions

In this study, hydraulic and seismic tomographic measurements were used to derive a site-specific relationship between the geophysical parameter p-wave velocity and the hydraulic parameters, diffusivity and specific storage. The database of the investigation is comprised of diffusivity tomograms derived from hydraulic travel time inversions, specific storage tomograms derived from hydraulic attenuation tomography and p-wave velocity tomogram derived from seismic tomography. The experimental set-up was designed such that the p-wave velocity tomograms overlap by half with the hydraulic tomograms. The diffusivity and specific storage tomograms were originally presented in Brauchler et al. [2011].

For the performance of seismic cross-well measurements, four non-permanent direct-push wells, with an inner diameter of 0.016 m, were installed and used as source wells. The non-permanent direct-push wells were chosen as source wells because conventional PVC-wells could possibly be damaged by the sparker source. For test initiation a modified p-wave sparker probe, SBS 42, adapted to small diameter wells in combination with an electric surge generator and a remote control unit was used. For the generation of the needed infrastructure direct-push technology shows a great deal of flexibility for the performance of high-resolution hydraulic or geophysical investigations in unconsolidated sediments. Test and observation points could be

installed with different types of casing materials and diameters, i.e. very efficient in terms of time, effort and finances.

The data integration, combining the results of the hydraulic and seismic tomograms, was realized by applying a procedure, which is based on k-means cluster analysis. The applied procedure enables us to transform the reconstructed p-wave velocity distribution of the seismic tomographic measurements into two zones with different hydraulic properties. In particular, the lateral and vertical changes of a zone, characterized by higher diffusivity and lower specific storage values, could be reconstructed.

The investigation showed that geophysical and hydraulic tomography complement one another because hydraulic tomography overcomes the problems of traditional hydrogeological measurements that generally do not provide high-resolution parameter estimates. The comparable spatial resolution of hydraulic and geophysical tomograms can be exploited to improve the potential of geophysical tomograms in the analysis of the spatial distribution of hydraulic properties. Hydraulic tomography can be used, for example, as a criterion in evaluating the individual expressiveness of the different geophysical methods, with respect to their capability in reconstruction of hydraulic significant structures from joint hydrogeophysical inversions. Such an assessment is difficult with conventional hydraulic and laboratory tests due to the low spatial resolution and uncertainty of the spatial assignment of the estimated hydraulic properties. Beyond this, the geophysical tomographic measurements allow for an easy extension of the area investigated with hydraulic tomography, since geophysical cross-well measurements could be performed more rapidly than hydraulic cross-well tests and thus, a larger area can be investigated in one array.

Acknowledgements

The investigations were partly conducted with the financial support of the German Research Foundation to the project “High resolution aquifer characterization based on direct-push technology: An integrated approach coupling hydraulic and seismic tomography,” under grant no. BR3379/1-2. For the allocation of parts of the seismic equipment we would like to thank Geotomographie GmbH. Joseph Doetsch was also partially funded by DOE-LBNL under contract number DE-AC02-05CH11231. Three anonymous reviews significantly helped to improve the quality of this paper.

References:

Archie, G. E. (1942) The electrical resistivity log as an aid in determining some reservoir characterisitics, Trans. Amer. Ins. Mining Metallurgical and Petroleum Engineers, 146, 54-62

Bohling, G. C., X. Zhan, J. J. Butler Jr., and L. Zheng (2002) Steady shape analysis of tomographic pumping tests for characterization of aquifer heterogeneous, Water Resour. Res., 38(12), 1324, doi: 10.1029/2001WR001176

Brauchler, R., R. Liedl, and P. Dietrich (2003) A travel time based hydraulic tomographic approach, Water Resour. Res., VOL. 39, NO. 12, 1370, doi:10.1029/2003WR002262.

Brauchler, R., J. Cheng, M. Everett, B. Johnson, P. Dietrich, R. Liedl, and M. Sauter (2007) An inversion strategy for hydraulic tomography: Coupling travel time and amplitude inversion. J. of Hydrol., doi:10.1016/j.jhydrol.2007.08.011.

Brauchler, R., R. Hu, T. Vogt, D. Halbouni, T. Heinrichs, T. Ptak, and M. Sauter (2010) Cross-well interference slug tests: An efficient tool for high resolution characterization of hydraulic heterogeneity. J. of Hydrol. 384, 33-45, doi:10.1016/j.jhydrol.2010.01.004.

Brauchler, R., R. Hu, P. Dietrich, and M. Sauter (2011) A field assessment of high-resolution aquifer characterization based on hydraulic travel time and hydraulic attenuation tomography, Water Resour. Res., 47, W03503, doi:10.1029/2010WR009635

Brauchler, R., Hu, R., Hu, L., Ptak, T. (2012) Bestimmung von hydraulischen Parametern in Lockergesteinen: Ein Vergleich unterschiedlicher Feldmethoden, Grundwasser, doi:10.1007/s00767-011-0185-6

Butler J.J., Jr. (1998) The Design, Performance, and Analysis of Slug Tests, Lewis Pub., 252 pp.

Butler Jr., J. J., C. D. McElwee and G. C. Bohling (1999) Pumping tests in networks of multilevel sampling wells: Motivation and methodology, Water Resources Research, 35(11), 3553-3560

Butler, J.J., Jr. (2005) Hydrogeological methods for estimation of hydraulic conductivity, in Hydrogeophysics, edited by Y. Rubin and S. Hubbard, Springer, Dordrecht

Butler, J.J., Jr. (2002) A simple correction for slug tests in small-diameter wells, Ground Water, v. 40, no. 3, pp. 303-307

Cardiff, M., Kitanidis, P., K. (2009) Bayesian inversion for facies detection: An extensible level set framework. Water Resources Research 45, W10416.

Cassiani, G., G. Böhm, A. Vesnaver, and R. Nicolich (1998) A geostatistical framework for incorporating seismic tomography auxiliary data into hydraulic conductivity estimation, J. Hydrol., 206, 58–74, doi:10.1016/S0022694(98)00084-5

Chen, J., S. Hubbard, and Y. Rubin (2001), Estimating the hydraulic conductivity at the South Oyster Site from geophysical tomographic data using Bayesian techniques based on the normal linear regression model, Water Resour. Res., 37(6), 1603–1613.

Chen, J., S. Hubbard, Y. Rubin, C. Murray, and E. Roden (2004), Geochemical characterization using geophysical data and Markov chain Monte Carlo methods: A case study at the South Oyster Bacterial Transport Site in Virginia, Water Resour. Res., 40, W12412, doi:10.1029/2003WR002883.

Cooper H.H., Jacob, C.E. (1946), A Generalized Graphical Method for Evaluation Formation Constants and Summarizing Well-Field History. Transactions, American Geophysical Union, 27(4), 526- 534.

Day-Lewis, F. D., and J. W. Lane Jr. (2004), Assessing the resolution-dependent utility of tomograms for geostatistics, Geophys. Res. Lett., 31, L07503, doi:10.1029/2004GL019617

Dietrich P., T. Fechner, J. Whittaker and G. Teutsch, An Integrated Hydrogeophysical Approach to Subsurface Characterization.- In: Herbert M., Kovar K. (Eds.): Groundwater Quality: Remediation and Protection, IAHS Publication No. 250, ISSN 0144-7815: 513-520, 1998.

Dietrich, P. and C. Leven (2006) Direct push technologies. In Groundwater Geophysics, ed. R. Kirsch, 321–340. Berlin, Heidelberg, Germany: Springer.

Dietrich, P. and Tronicke, J. (2009) Integrated analysis and interpretation of cross-hole P- and S-wave tomograms: a case study. Near Surface Geophysics, 7, 101-109. doi: 10.3997/1873-0604.2008041.

Doetsch, J., N. Linde, I. Coscia, S. A. Greenhalgh, and A. G. Green (2010), Zonation for 3D aquifer characterization based on joint inversions of multimethod crosshole geophysical data, Geophysics 75, G53, doi:10.1190/1.3496476

Eppstein, M.J. and D.E. Dougherty (1998) Optimal 3-D Traveltime Tomography, Geophysics, 63, 1053, doi:10.1190/1.1444383

Ferré, T., L. Bentley, A. Binley, N. Linde, A. Kemna, K. Singha, K. Holliger, J. A. Huisman, and B. Minsley (2009) Critical steps for the continuing advancement of hydrogeophysics. EOS Transactions, American Geophysical Union, 90, 200.

Gallardo, L. A., and M. A. (2003), Characterization of heterogeneous near-surface materials by joint 2Dinversion of dc resistivity and seismic data, Geophys. Res. Lett. 30, 1658, doi:10.1029/2003GL017370

Gilbert, P. (1972) Iterative methods for three-dimensional reconstruction of an object from projections. J. Theor. Biol. 36, 105-117.

Gottlieb, J. and P. Dietrich (1995) Identification of the permeability distribution in soil by hydraulic tomography.- Inverse Problems, 11: 353-360.

Hsieh, P. A., S. P., Neuman, G. K. Stiles, and E. S. Simpson (1985), Field determination of the three-dimensional hydraulic conductivity tensor of anisotropic media: 2. Methodology and application to fractured rocks, Water Resources Research, 21, 1667-1676.

Hu, R., Brauchler, R., Herold, M. and P. Bayer. (2011) Hydraulic tomography analogue study: Coupling travel time and steady shape inversion, Journal of Hydrology, 409, (1-2), 350-362, 10.1016/j.jhydrol.2011.08.031

Hu, R. (2011) Hydraulic tomography: a new approach coupling hydraulic travel time, attenuation and steady shape inversions for high-spatial resolution aquifer characterization, Hochschulschrift: Göttingen, Univ., Diss., 116 S.

Huggenberger, P., Regli, C. (2006) A sedimentological model to characterize braided river deposits for hydrogeological applications. In: Sambrook-Smith G, Best J, Bristow C, Petts G (eds) Braided Rivers, Process, Deposits, Ecology and Management. ISA Special Publication 36:51-74.

Hubbard, S. S., Y. Rubin, and E. Majer (1999) Spatial correlation structure estimation using geophysical and hydrogeological data, Water Resour. Res., 35(6), 1809–1825, doi:10.1029/1999WR900040

Hinnell, A. C., T. Ferré, J. A. Vrugt, J. A. Huisman, S. Moysey, J. Rings, and M. B. Kowalsky (2010) Improved extraction of hydrologic information from geophysical data through coupled hydrogeophysical inversion, Water Resour. Res., 46, doi:10.1029/2008WR007060, 2010

Hyndman, D. W., Harris, J. M., Gorelick, S. (1994). Coupled seismic and tracer test inversion for aquifer property characterization. Water Resources Research 30(7): doi: 10.1029/94WR00950

Hyndman, D. W., Harris, J. M. (1996) Traveltime inversion for the geometry of aquifer lithologies, Geophysics, 61(6), 1728–1737

Hyndman, D. W., J. R. Harris, and S. M. Gorelick (2000), Inferring the relation between seismic slowness and hydraulic conductivity in heterogeneous aquifers, Water Resour. Res., 36(8), 2121–2132.

Hyndman, D. W., and J. Tronicke (2005) Hydrogeophysical case studies at the local scale: The saturated zone, in Hydrogeophysics, edited by Y. Rubin and S. Hubbard, Springer, Dordrecht

Illman, W.A., J. Zhu, A.J. Craig, and D. Yin (2010) Comparison of aquifer characterization approaches through steady state groundwater model validation: A controlled laboratory sandbox study, Water Resour. Res., 46, W04502, doi:10.1029/2009WR007745.

Jackson M.J. and D.R. Tweeton (1996) 3DTOM: Three-dimensional Geophysical Tomography. United States Department of the Interior, Bureau of Mines, Report of Investigation 9617, 84 pp.

Karasaki, K., B. Friefeld, A. Cohen, K. Grossenbacher, P. Cook, and D. Vasco (2000), A multi-disciplinary fractured rock characterization study at the Raymond field site, Raymond, California, Journal of Hydrology, 236, 17-34

Kowalsky, M. B., S. Finsterle, and Y. Rubin (2004), Estimating flow parameter distributions using ground-penetrating radar and hydrological measurements during transient flow in the vadose zone, Adv. Water Resour., 27(6), 583–599

Kowalsky, M., S. Finsterle, J. Peterson, S. Hubbard, Y. Rubin, E. Majer, A. Ward, and G. Gee (2005), Estimation of field-scale soil hydraulic parameters and dielectric parameters through joint inversion of GPR and hydrological data, Water Resour. Res., 41, W11425, doi:10.1029/2005WR004237

Leven, C. and Dietrich, P. (2006) What information can we get from pumping tests?-comparing pumping test configurations using sensitivity coefficients, J. of Hydrol. 319 (1-4), 199-215

Linde, N., A. Binley, A. Tryggvason, L. B. Pedersen, and A. Revil (2006a), Improved hydrogeophysical characterization using joint inversion of cross-hole electrical resistance and ground-penetrating radar traveltime data, Water Resources Research, 42(12), W12404, doi:10.1029/2006WR005131.

Linde, N., S. Finsterle, and S. Hubbard (2006b), Inversion of tracer test data using tomographic constraints, Water Resour. Res., 42, W04410, doi:10.1029/2004WR003806

McQueen, J. (1967) Some methods for classification and analysis of multivariate observations, in Proceedings of the Fifth Berkeley Symposium on Mathematics, Statistics and Probability, 1, pp. 281– 298, Univ. of California, Berkeley.

Melville, J.G., Molz, F.J., Guven, O., and M.A. Widdowson, 1991, Multilevel slug tests with comparison to tracer data, Ground Water, 29(6), 897-907.

Ni, C.F., T.-C. J. Yeh, 2008, Stochastic inversion of pneumatic cross-hole tests and barometric pressure fluctuations in heterogeneous unsaturated formations, Advances in Water Resources, Volume: 31, Issue: 12 Pages: 1708-1718

Paasche, H., J. Tronicke, K. Holliger, A.G. Green, and H. Maurer (2006) Integration of diverse physical-property models: Subsurface zonation and petrophysical parameter estimation based on fuzzy *c*-means cluster analyses. *Geophysics*, 71

Paasche, H., J. Tronicke, and P. Dietrich, P. (2010) Automated integration of partially colocated models: subsurface zonation using a modified fuzzy c-means cluster algorithm. *Geophysics,* 75

Straface, S., T.-C.J Yeh, J. Zhu, S. Troisi, and C.H. Lee (2007) Sequential aquifer tests at a well field, Montalto Uffugo Scalo, Italy, Water Resources Research, 43, W07432, doi:10.1029/2006WR005287.

Topp, G.C., J.L. Davis, and A.P. Annan (1980) Electromagnetic determination of soil water content: Measurements in coaxial transmission lines, Waster Resour. Res., 16, 547-582

Tronicke, J., K. Holliger, W. Barrash, and M. D. Knoll (2004), Multivariate analysis of cross-hole georadar velocity and attenuation tomograms for aquifer zonation, Water Resour. Res., 40, W01519, doi:10.1029/2003WR002031

Vasco, D.W. H. Keers, and K. Karasaki (2000) Estimation of reservoir properties using transient pressure data: An asymptotic approach, Water Resources Res., 36(9), 3447-3465.

Vasco, D.W., and K. Karasaki (2001), Inversion of pressure observations: an integral formulation, Journal of Hydrology, 253, 27-40.

Virieux, J., C. Flores-Luna, and D. Gibert (1994) Asymptotic theory for diffusive electromagnetic imaging, Geophys. J. Int., 119, 857–868.

Wu, C.-M., T.-C. J. Yeh, J. Zhu, T.H. Lee, N.-S. Hsu, C.-H. Chen, C.-H., and A.F. Sancho (2005) Traditional analysis of aquifer tests: Comparing apples to oranges?, Water Resour. Res., 41, W09402, doi:10.1029/2004WR003717.

Xiang J., T.-C. J. Yeh, C.-H. Lee, K.-C. Hsu, J.-C. Wen (2009), A simultaneous successive linear estimator and a guide for hydraulic tomography analysis, Water Resour. Res., 45, W02432, doi:10.1029/2008WR007180

Yeh, T.-C.J. and S. Liu (2000) Hydraulic tomography: Development of a new aquifer test method, Water Resources Research 36 (8), 2095-2105

Yeh, T.-C. J., S. Liu, R. J. Glass, K. Baker, J. R. Brainard, D. Alumbaugh, and D. LaBrecque (2002), A geostatistically based inverse model for electrical resistivity surveys and its applications to vadose zone hydrology, Water Resour. Res., 38(12), 1278, doi:10.1029/2001WR001204

Yin, D. and W. A. Illman (2009) Hydraulic tomography using temporal moments of drawdown recovery data: A laboratory sandbox study, Water Resour. Res., 45, W01502, doi:10.1029/2007WR006623

Zhu, J., and T.-C. J. Yeh (2005), Characterization of aquifer heterogeneity using transient hydraulic tomography, Water Resour. Res., 41, W07028, doi:10.1029/2004WR003790

Zhu, J., and T.-C. J. Yeh (2006), Analysis of hydraulic tomography using temporal moments of drawdown recovery data, Water Resour. Res., 42, W02403, doi:10.1029/2005WR004309.

Table 1: Comparison of the RMSE of the p-wave velocity, diffusivity and specific storage tomograms with and without constraints.

	Tomogram (North – South direction)	Tomogram (West – East direction)
RMSE of p-wave velocity tomogram without constrain [µs]	3.32×10^{-2}	4.59×10^{-2}
RMSE of p-wave velocity tomogram with constrain [µs]	3.58×10^{-2}	5.96×10^{-2}
RMSE of diffusivity tomogram without constrain [s]	5.8×10^{-1}	5.3×10^{-1}
RMSE of diffusivity tomogram with constrain [s]	6.0×10^{-1}	6.2×10^{-1}
RMSE of specific storage tomogram without constrain [-]	2.17×10^{-2}	1.68×10^{-2}
RMSE of specific storage tomogram with constrain [-]	2.29×10^{-2}	2.09×10^{-2}

Figure 1: Well network at the Stegemühle site.

Figure 2: a) Reconstructed diffusivity tomogram. b) Reconstructed specific storage tomogram. The tomograms are taken from Brauchler et al. [2011]. c) Top view of the spatial position of the wells used for the cross-well slug interference tests.

Figure 3: Typical raw data gathers for a source depth of 5.06 m. Red dots represent the picked first arrivals. Although the seismic data were clipped, first arrivals could be picked reliably.

Figure 4: Tomographic measurement of five-star point set-up. Illustration of the measured source–receiver configurations. The hydraulic tests are displayed in black and the seismic measurement in pink.

Figure 5: Flowchart of the entire derivation of a site-specific relationship between hydraulic parameters and p-wave velocity.

Figure 6: Tomograms reconstructed in North-South direction. a) Reconstructed diffusivity tomogram. b) Reconstructed specific storage tomogram. c) Reconstructed p-velocity tomogram. d) Interpretation of the tomograms based on a zonation approach.

Figure 7: Tomograms reconstructed in East-West direction. a) Reconstructed diffusivity tomogram. b) Reconstructed specific storage tomogram. c) Reconstructed

p-velocity tomogram. d) Interpretation of the tomograms based on a zonation approach.

Figure 8: Scatterplots between the hydraulic properties, diffusivity and specific storage, and the geophysical property p-wave velocity. (a-b) Scatterplots recorded in North-South direction. (c-d) Scatterplots recorded in East-West direction.

Figure 9: Variograms derived from the diffusivity, specific storage and p-wave velocity tomograms performed in North-South (a-c) and West-East direction (d-f).

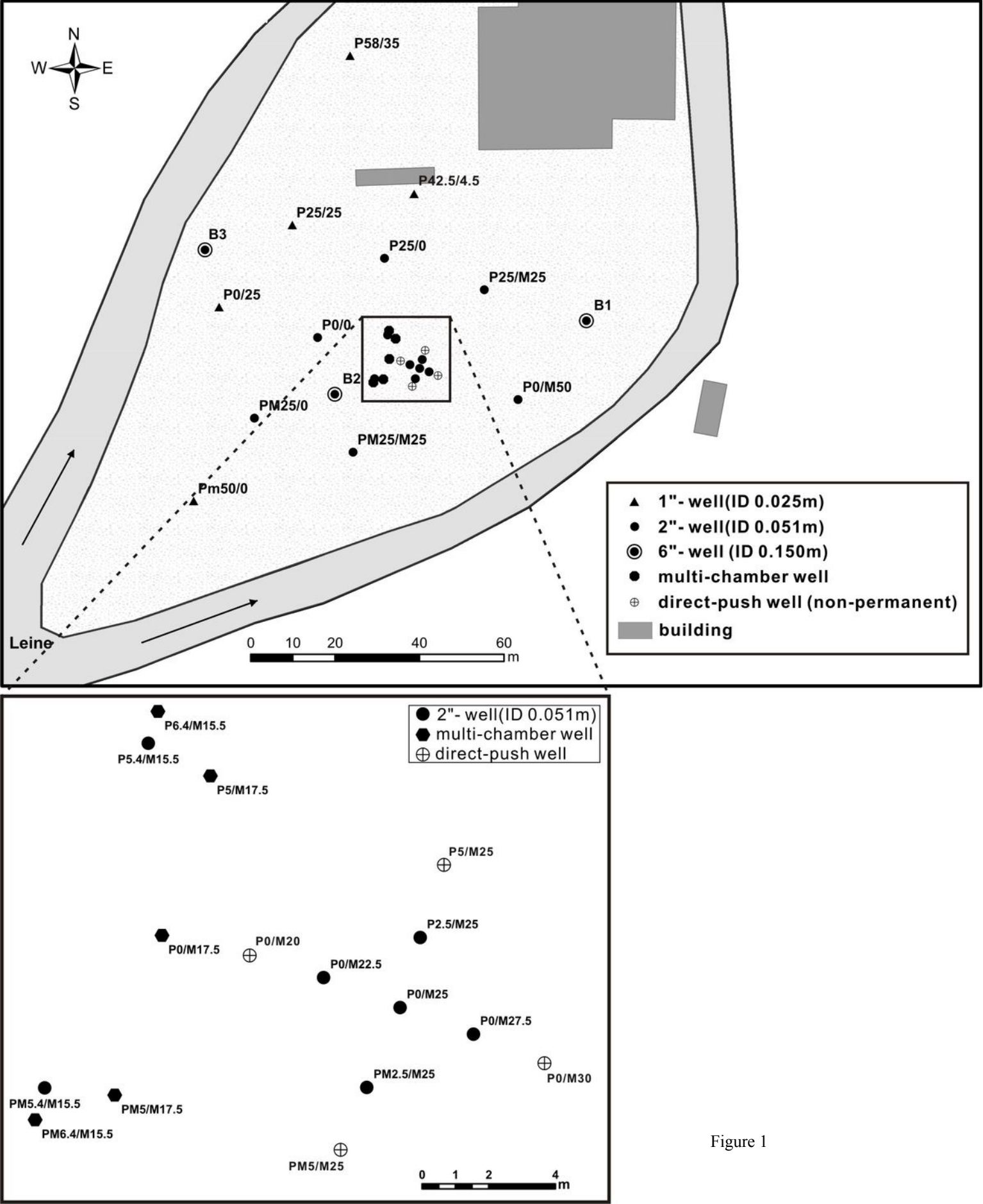
N
W
E
S
P58/35
P42.5/4.5
P25/25
B3
P25/0
P25/M25
P0/25
B1
P0/0
B2
P0/M50
PM25/0
PM25/M25
Pm50/0
Leine
0 10 20 40 60
m
1"- well(ID 0.025m)
2"- well(ID 0.051m)
6"- well (ID 0.150m)
multi-chamber well
direct-push well (non-permanent)
building
P6.4/M15.5
P5.4/M15.5
P5/M17.5
P5/M25
P2.5/M25
P0/M17.5
P0/M20
P0/M22.5
P0/M25
P0/M27.5
P0/M30
PM2.5/M25
PM5.4/M15.5
PM5/M17.5
PM6.4/M15.5
PM5/M25
0 1 2 4
m
2"- well(ID 0.051m)
multi-chamber well
direct-push well

Figure 1

(a) Diffusivity tomogram

(b) Specific storage tomogram

(c) Spatial position of the wells, top view

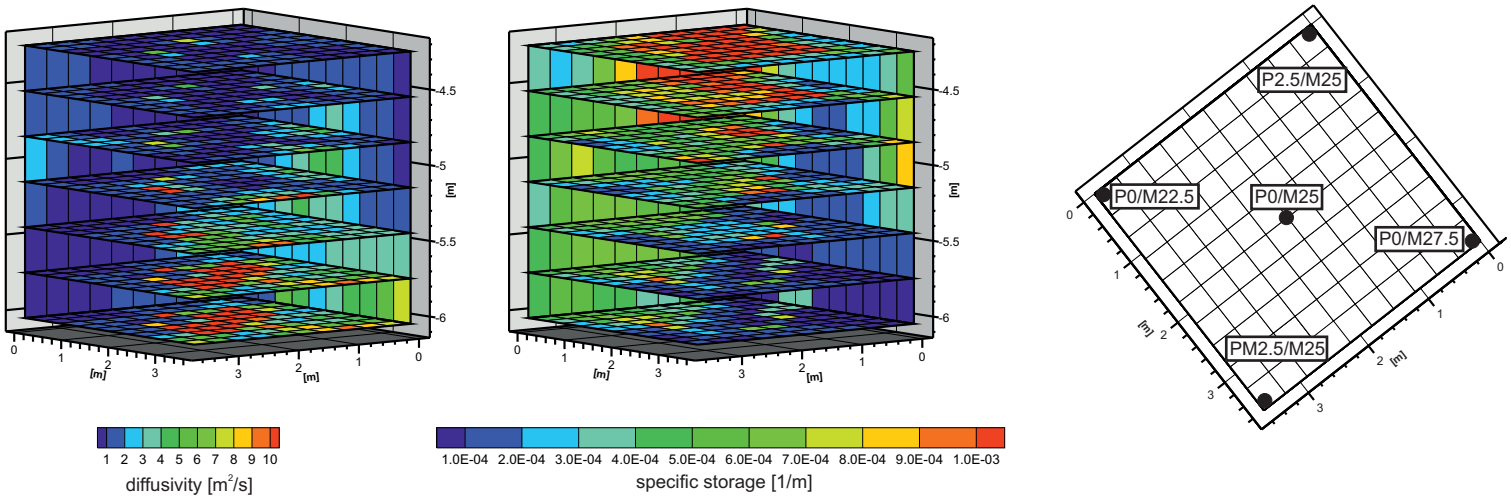

Figure 2

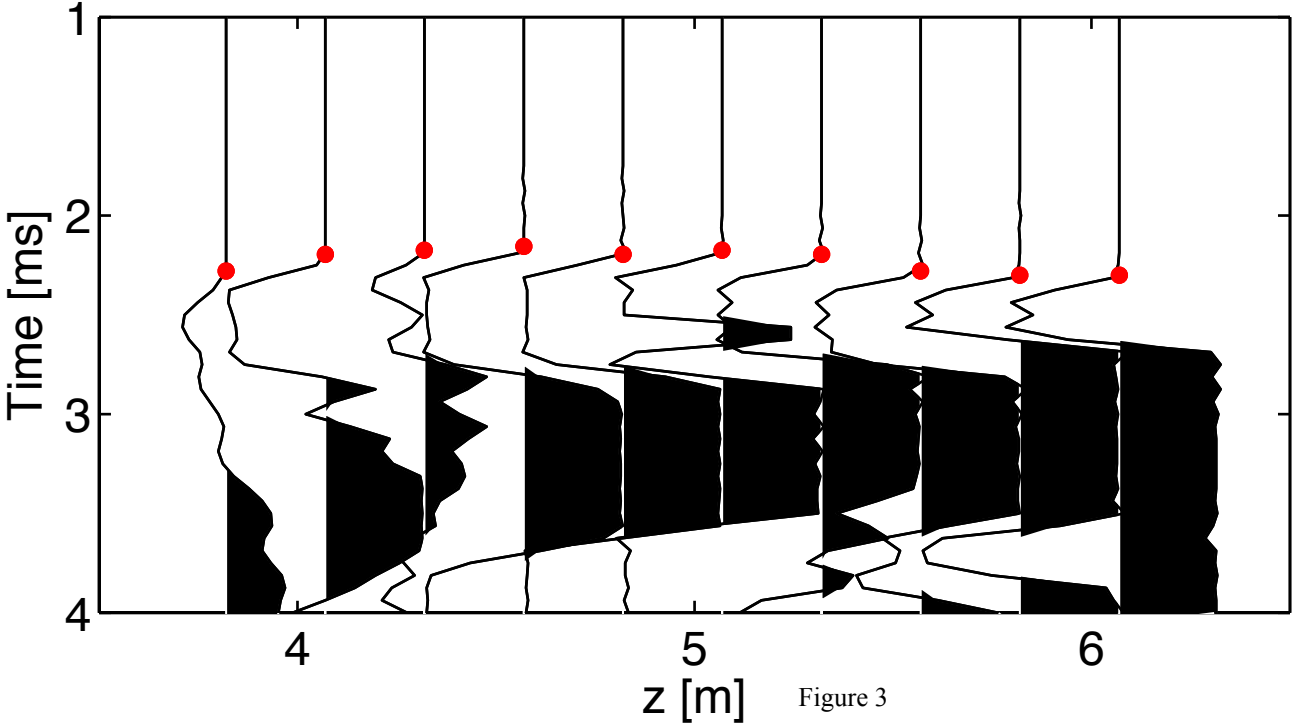

Figure 3

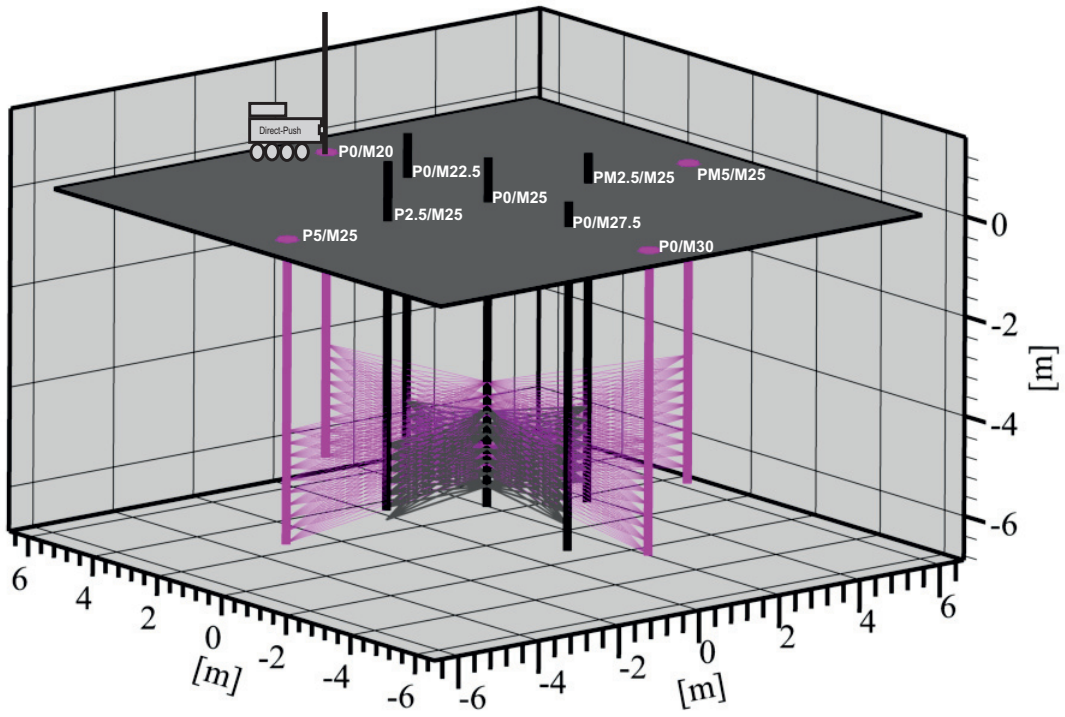
Direct-Push
P0/M20
P0/M22.5
P0/M25
P2.5/M25
P5/M25
PM2.5/M25
PM5/M25
P0/M27.5
P0/M30
0
-2
-4
-6
[m]
6
4
2
0
-2
-4
-6
[m]

Figure 4

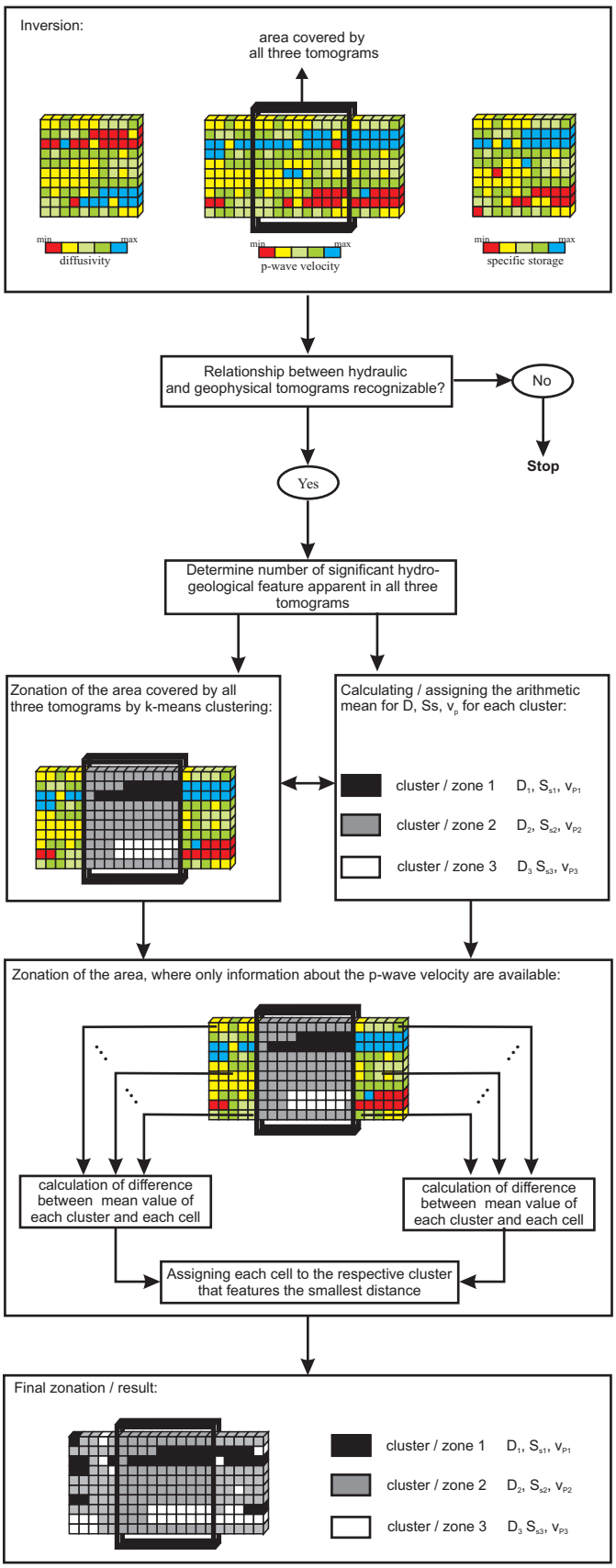
Inversion:
area covered by all three tomograms
min
max
diffusivity
min
max
p-wave velocity
min
max
specific storage
Relationship between hydraulic and geophysical tomograms recognizable?
No
Stop
Yes
Determine number of significant hydro-geological feature apparent in all three tomograms
Zonation of the area covered by all three tomograms by k-means clustering:
Calculating / assigning the arithmetic mean for D, Ss, v_p for each cluster:
cluster / zone 1 D1, Ss1, vP1
cluster / zone 2 D2, Ss2, vP2
cluster / zone 3 D3 Ss3, vP3
Zonation of the area, where only information about the p-wave velocity are available:
calculation of difference between mean value of each cluster and each cell
calculation of difference between mean value of each cluster and each cell
Assigning each cell to the respective cluster that features the smallest distance
Final zonation / result:
cluster / zone 1 D1, Ss1, vP1
cluster / zone 2 D2, Ss2, vP2
cluster / zone 3 D3 Ss3, vP3

Figure 5

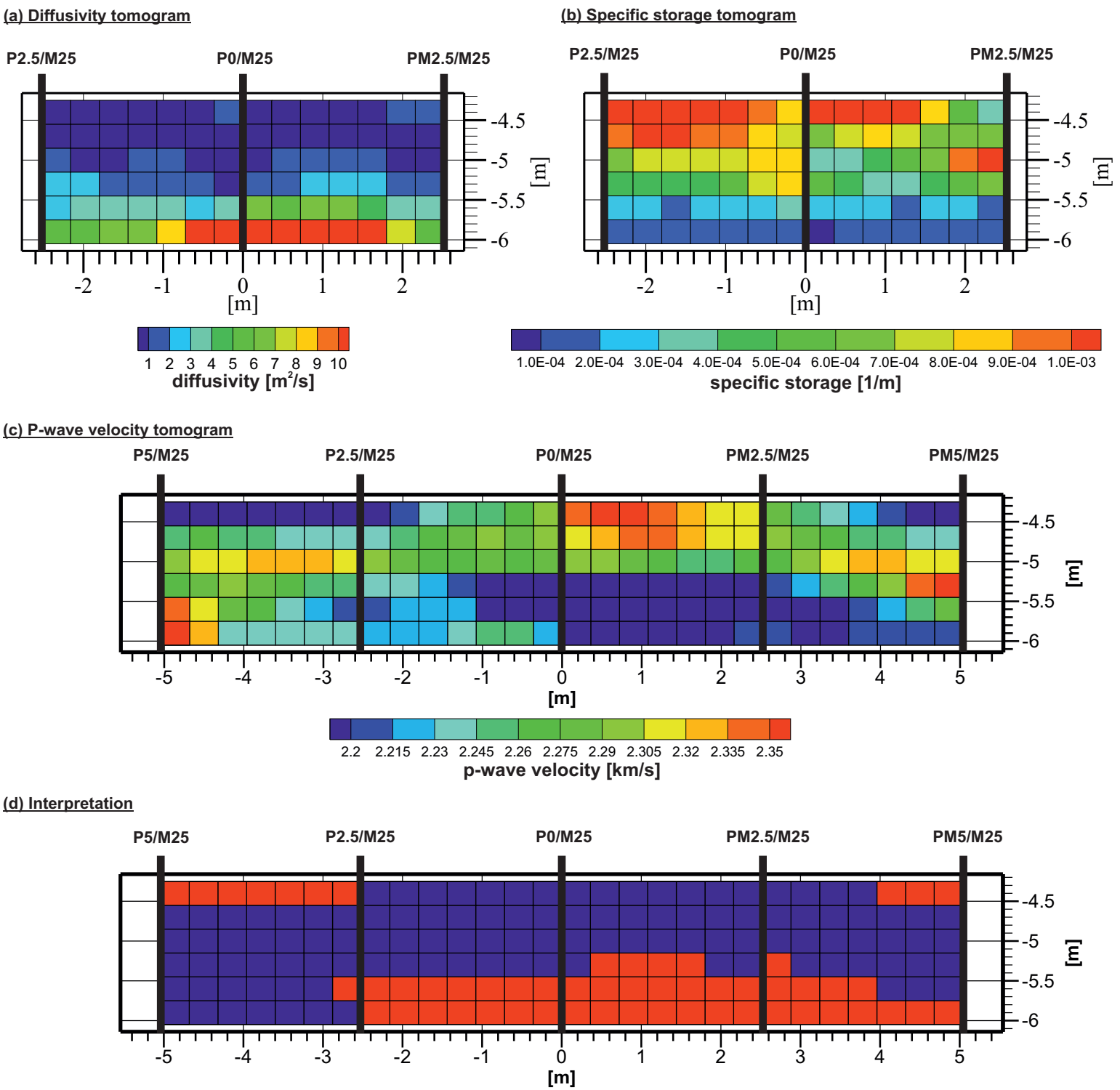
(a) Diffusivity tomogram
P2.5/M25
P0/M25
PM2.5/M25
-4.5
-5
-5.5
-6
[m]
-2
-1
0
1
2
[m]
1 2 3 4 5 6 7 8 9 10
diffusivity [m²/s]
(b) Specific storage tomogram
P2.5/M25
P0/M25
PM2.5/M25
-4.5
-5
-5.5
-6
[m]
-2
-1
0
1
2
[m]
1.0E-04 2.0E-04 3.0E-04 4.0E-04 5.0E-04 6.0E-04 7.0E-04 8.0E-04 9.0E-04 1.0E-03
specific storage [1/m]
(c) P-wave velocity tomogram
P5/M25
P2.5/M25
P0/M25
PM2.5/M25
PM5/M25
-4.5
-5
-5.5
-6
[m]
-5
-4
-3
-2
-1
0
1
2
3
4
5
[m]
2.2 2.215 2.23 2.245 2.26 2.275 2.29 2.305 2.32 2.335 2.35
p-wave velocity [km/s]
(d) Interpretation
P5/M25
P2.5/M25
P0/M25
PM2.5/M25
PM5/M25
-4.5
-5
-5.5
-6
[m]
-5
-4
-3
-2
-1
0
1
2
3
4
5
[m]
zone 1:
- K: 10-3 m/s
- Ss: 2×10-4 m-1
zone 2:
- K: 7×10-4 m/s
- Ss: 7×10-4 m-1

Figure 6

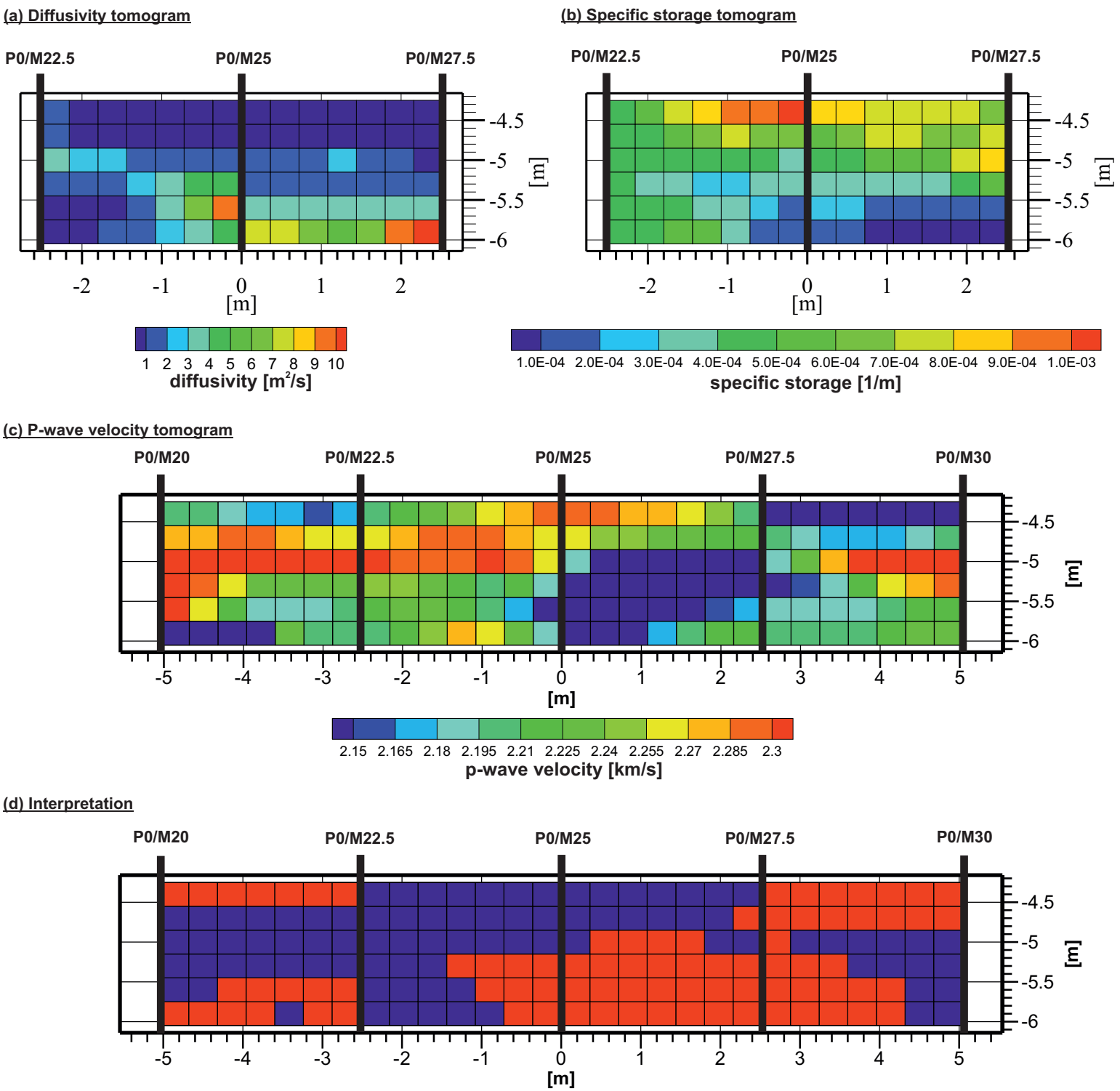
(a) Diffusivity tomogram
P0/M22.5
P0/M25
P0/M27.5
-4.5
-5
-5.5
-6
[m]
-2
-1
0
1
2
[m]
1 2 3 4 5 6 7 8 9 10
diffusivity [m²/s]
(b) Specific storage tomogram
P0/M22.5
P0/M25
P0/M27.5
-4.5
-5
-5.5
-6
[m]
-2
-1
0
1
2
[m]
1.0E-04 2.0E-04 3.0E-04 4.0E-04 5.0E-04 6.0E-04 7.0E-04 8.0E-04 9.0E-04 1.0E-03
specific storage [1/m]
(c) P-wave velocity tomogram
P0/M20
P0/M22.5
P0/M25
P0/M27.5
P0/M30
-4.5
-5
-5.5
-6
[m]
-5
-4
-3
-2
-1
0
1
2
3
4
5
[m]
2.15 2.165 2.18 2.195 2.21 2.225 2.24 2.255 2.27 2.285 2.3
p-wave velocity [km/s]
(d) Interpretation
P0/M20
P0/M22.5
P0/M25
P0/M27.5
P0/M30
-4.5
-5
-5.5
-6
[m]
-5
-4
-3
-2
-1
0
1
2
3
4
5
[m]
zone 1:
- K: 10-3 m/s
- Ss: 2×10-4 m-1
zone 2:
- K: 7×10-4 m/s
- Ss: 7×10-4 m-1

Figure 7

Scatterplots (North-South direction):

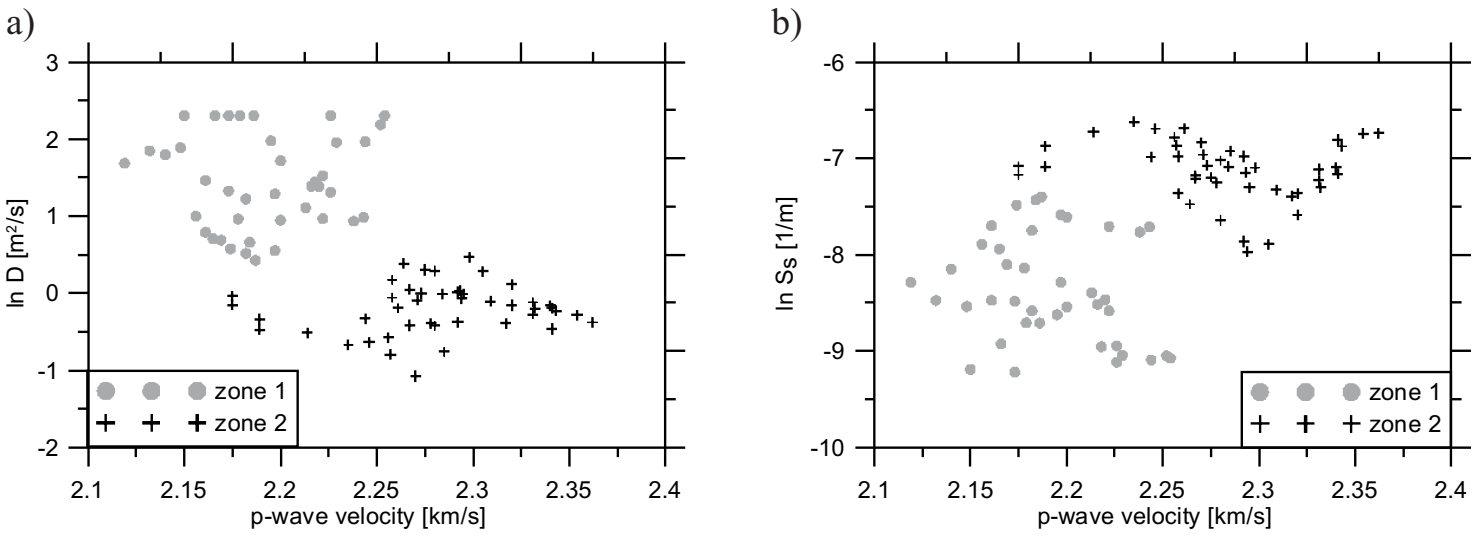

Scatterplots (East-West direction):

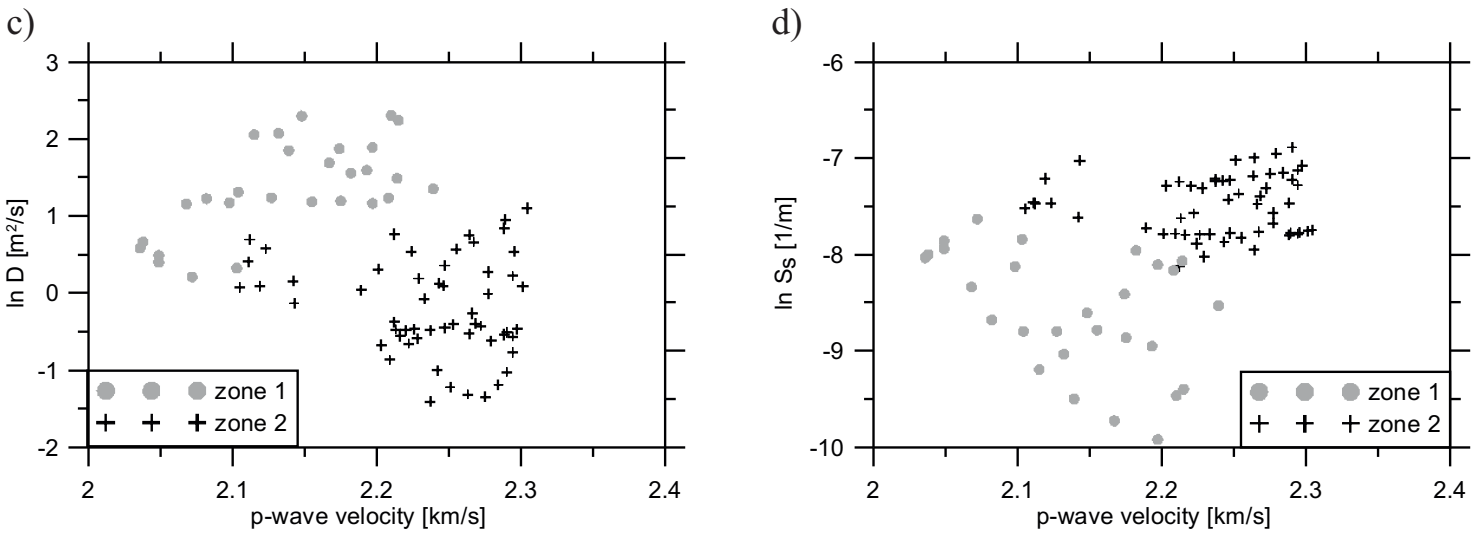

Figure 8

(a) Variogram of the diffusivity between wells P2.5/M25 and PM2.5/M25

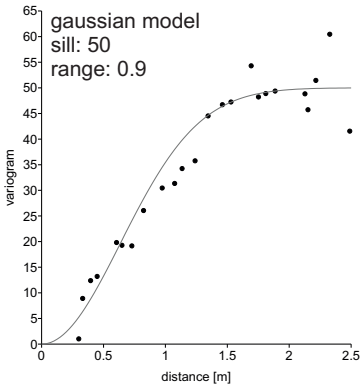

(b) Variogram of the specific storage between wells P2.5/M25 and PM2.5/M25

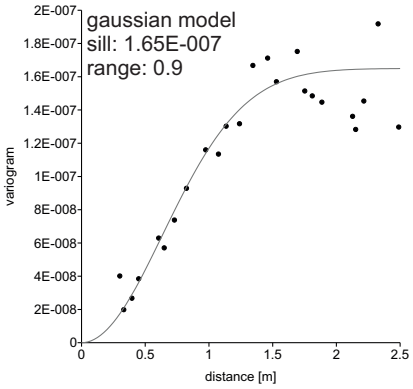

(c) Variogram of the p-wave velocity between wells P2.5/M25 and PM2.5/M25

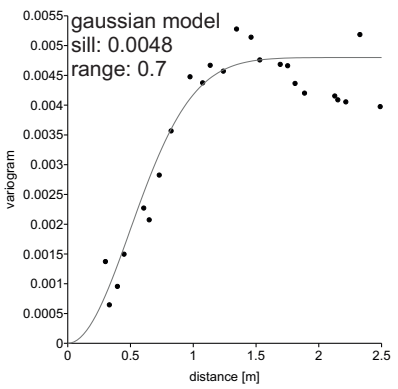

(d) Variogram of the diffusivity between wells P0/M22.5 and P0/M27.5

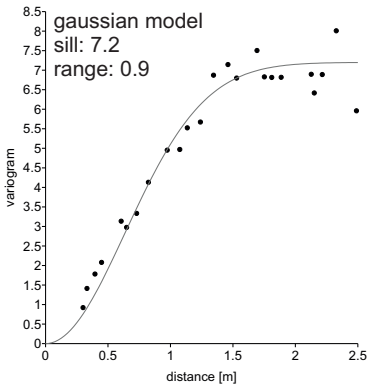

(e) Variogram of the specific storage between wells P0/M22.5 and P0/M27.5

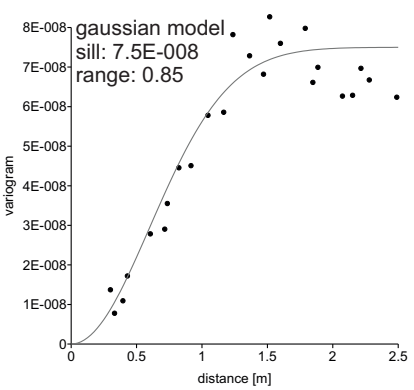

(f) Variogram of the p-wave velocity between wells P0/M22.5 and P0/M27.5

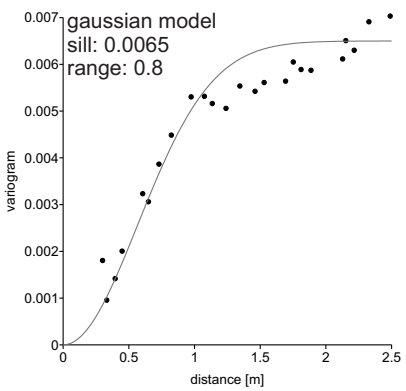

Figure 9